agriculture

Article

A Method to Study the Influence of the Pesticide Load on the Detailed Distribution Law of Downwash for Multi-Rotor UAV

Fengbo Yang [1,2], Hongping Zhou [1,2,*], Yu Ru [1,2], Qing Chen [1,2] and Lei Zhou [1,2]

[1] Co-Innovation Center of Efficient Processing and Utilization of Forest Resources, Nanjing Forestry University, Nanjing 210037, China
[2] College of Mechanical and Electronic Engineering, Nanjing Forestry University, Nanjing 210037, China
* Correspondence: hpzhou@njfu.edu.cn

Abstract: Multi-rotor plant protection Unmanned Aerial Vehicles (UAVs) have suitable terrain adaptability and efficient ultra-low altitude spraying capacity, which is a significant development direction in efficient plant protection equipment. The interaction mechanisms of the wind field, droplet, and crop are unclear, and have become the bottleneck factor restricting the improvement of the deposition quality. This paper suggests a method to study the influence of the pesticide load on the detailed distribution law of downwash for a six-rotor UAV. Based on a hexahedral structured mesh, a 3D numerical calculation model was established. Analysis showed that the relative errors between the simulated and measured velocities in the *z*-axis were less than 11% when the downwash air flow was stable. Numerical simulations were carried out for downwash in hover under 0, 1, 2, 3, 4, and 5 kg loads. The effect of load on the airflow was evident, and the greater the load was, the higher the wind speed of downwash would be. Then, the influence of wing interference on the distribution of airflow would be more pronounced. Furthermore, under the rotation of the rotor and the extrusion of external atmospheric pressure, the "trumpet" phenomenon appeared in the downwash airflow area. As an extension, the phenomenon of the "shrinkage–expansion" was shown in the longitudinal section under heavy load, while the phenomenon of "shrinkage–expansion–shrinkage" was present under light load. After that, based on the detailed analysis of the downwash wind field, the spray height of this multi-rotor UAV was suggested to be 2.5 m or higher, and the nozzle was recommended to be mounted directly under the rotor and to have the same rotation direction as the rotor. The research in this paper lays a solid foundation for the proposal of the three-zone overlapping matching theory of wind field, droplet settlement, and canopy shaking.

Keywords: UAV; pesticide load; downwash; numerical simulation; controlled testing

check for updates

Citation: Yang, F.; Zhou, H.; Ru, Y.; Chen, Q.; Zhou, L. A Method to Study the Influence of the Pesticide Load on the Detailed Distribution Law of Downwash for Multi-Rotor UAV. *Agriculture* **2022**, *12*, 2061. https://doi.org/10.3390/agriculture12122061

Academic Editor: Yubin Lan

Received: 12 October 2022
Accepted: 25 November 2022
Published: 1 December 2022

1. Introduction

Multi-rotor plant protection UAV, which has broken through the limitations of crop and operation types, has a technical ability that manual and traditional agricultural machinery plant protection operations cannot match [1,2]. In recent years, UAVs have captured a great deal of attention [3,4], and have been applied to the military field, rescue and disaster relief, and agricultural fields such as seeding, spraying, and fertilization. In the context of China's strategic goals of "clean water and green mountain is gold", the No. 1 central document in 2021 emphasizes the implementation of the "agricultural green development strategy", and the promotion of "green technology and equipment for the prevention and control of the crop pests and diseases" as particularly important [5]. With the rural labor market gradually shrinking, plant protection machinery is facing the dual pressures of ensuring yield and green safety. Therefore, multi-rotor plant protection UAV has become the best choice for dispersed plots and hilly mountains [1]. As of the second half of 2020, the number of plant protection UAVs in China is about 80,000, and the annual operation area is nearly 533.33 billion square meters. The aerial pesticide application represented by multi-rotor plant protection UAV spray has become one of the key development directions of efficient plant protection machinery and precision pesticide application technology in China [6].

In the background of aerial pesticide application, affected by multiple factors such as combined wind field and crop canopy, the drift, settlement, and deposition of spray droplets between crops is a complex interactive physical processes. To improve the spray effect of human-crewed aircraft and ground machinery, and promote the optimization design of plant protection machinery, drift and deposition models such as AGDISP and AgDRIFT have been developed and improved by international scholars [7]. Studies have shown that the drift buffer distance and deposition uniformity of multi-rotor plant protection UAVs are significantly different from those of ground machinery and single-rotor helicopters [8,9]. The low-altitude and low-volume spray method make the coupling effects of the combined wind field, droplets, crop canopy, and meteorological environment complex, and the existing international mature drift and deposition models cannot be directly and effectively applied to our country's small multi-rotor plant protection UAV [10]. Droplet drift and canopy deposition uniformity under combined wind field–pesticide droplet–crop canopy interaction are significant typical problems faced by aerial spraying, as shown in Figure 1. Based on field spray experiments, scholars have discussed the influence of many factors (model and spray mechanism of UAV, spray parameters, crop types, meteorological factors, etc.) on the spray drift and deposition characteristics of the multi-rotor plant protection UAV. Still, there is room for correction with regard to these studies [11,12]. At the same time, researchers face problems such as unstable and uncontrollable meteorological factors, too large coefficients of variation, and unrepeatable test results, which make it difficult to scientifically evaluate the spray effect of plant protection UAVs solely through field experiments [13]. Given this, some scholars have developed a particular wind tunnel, developed a multi-rotor platform that can spray horizontally and vertically, reproduced the flying spray conditions in a laboratory environment, and studied the relationship between deposition quality and various factors [14]. Some studies have also established and verified the spraying drift and deposition models of some rotor plant protection UAVs by combining computational fluid dynamics (CFD) and laboratory experiments [15,16]. In general, on the one hand, the field meteorological environment changes instantaneously, the accuracy of field experiments is not high, and the preliminary experimental models of droplet drift and canopy deposition cannot directly characterize the spray effect. On the other hand, the theoretical model constructed based on repeated indoor spray experiments in the field lacks the complete characteristics of the crop canopy, and ignores the interaction of combined wind field, spray droplets, crop canopy, spray parameters, meteorological environment on droplet drift and canopy deposition. Under the stress of the combined wind field, the droplets are transported to the crop area directionally, the crops shift laterally, the transverse porosity of the canopy increases significantly, the deposition on the back of leaves increases significantly, and the longitudinal deposition uniformity of crops is improved [17,18]. It can be seen that the wind field is a crucial factor affecting the deposition level of multi-rotor plant protection drones [19].

Derrick, Yeo, et al. [20] pointed out that proximity operations of small rotary wing air vehicles posed a unique challenge due to the downwash, and they presented a downwash detection and localization strategy intended for use with small rotorcraft. To predict the rotorcraft motion in the vicinity of objects or their wake, a real-time capable model was presented by J. Bludau, et al. [21]. In this model, the UAV was modeled by wall boundary conditions in the Lattice–Boltzmann method and updated dynamically at every time step. Then, the two-way coupled simulation enabled the prediction of the rotorcraft motion and flight dynamics in arbitrary situations without prior knowledge of the flow field. Generally speaking, relatively actual wind field data can be obtained when the test conditions are controllable, and the assumptions of theoretical calculations are reasonable. However, in the field of aviation plant protection, we not only need to research the distribution regularity of the downwash, but also the interaction of wind field–canopy and wind field–fog droplets; moreover, and it is extremely difficult to analyze purely by testing and theoretical calculations. The CFD technique happens to be fully utilized to achieve it [15]. In the plant protection field, CFD was first applied to simulate the orchard spraying process [22–24]. However, CFD technology has continued to be involved in the aviation spray field in recent years. Bin Zhang et al. [25] used CFD techniques to study the velocity field of the wake of a Thrush 510G (Africair, Inc., Miami, FL, USA) close to the ground. CFD techniques were also used to predict the velocity field and the subsequent trajectories of spray droplets in the wake of a Thrush 510G aircraft [26]. Through the CFD method, we can observe the movement and distribution law of the wind field and droplet group in real-time, which is incomparable to the experimental analysis.

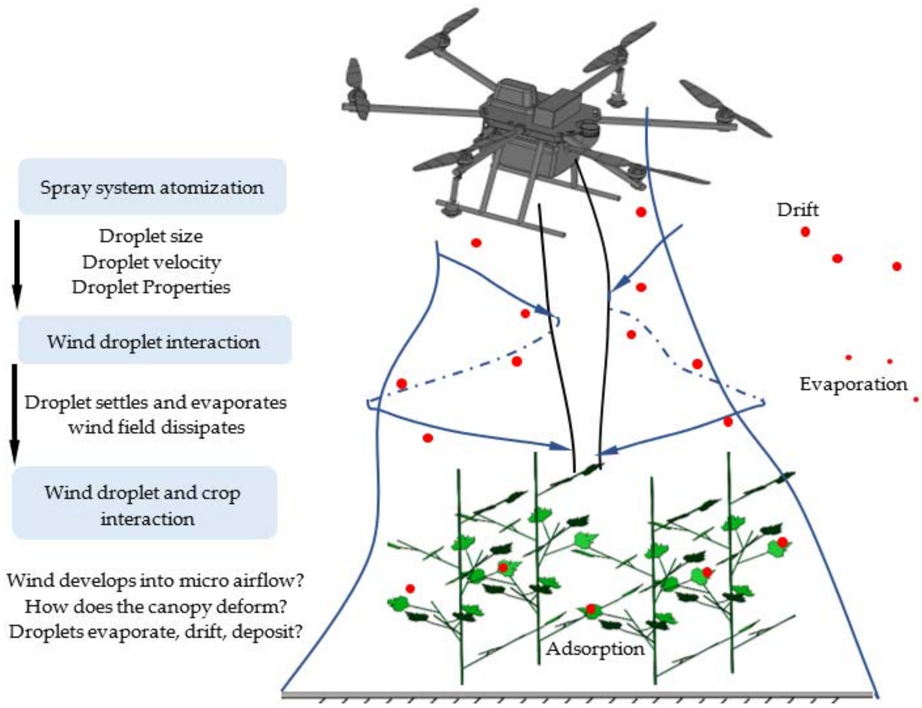

Figure 1. Schematic diagram of flight pesticide application of multi-rotor plant protection UAV.

The downwash drives the droplets to move, evaporate, settle, and drift, while the airflow intensity attenuates; the downwash forces the stems, branches, and leaves to bend, and the strong airflow develops into a micro airflow. Downwash is a crucial factor affecting the deposition level of multi-rotor plant protection UAVs, and it is the focus of this study. Numerical simulations will be carried out for the downwash under different loads using CFD tools. The downwash distribution of the horizontal and vertical cross-sections at different heights will be analyzed in detail. In this way, we can clarify the development law of the downwash flow in adjacent rotors and opposite rotors at different heights. Then, UAV operation parameters can be better determined, including the relative position of nozzles on UAVs to ensure the downwash can drive the droplets in the whole process and the height of flight to strengthen the shaking of the canopy under the premise of safety.

2. UAV Research Models and Methods

2.1. Physical Structure Model

The scanning process of the vital execution component of a six rotor plant protection UAV is shown in Figure 2, which was completed by Optimscan5-2015011K05. After the calibration of the Optimscan5-2015011K05 and the marking of the typical feature points of the rotor, multiple scanning surfaces were positioned through the reference plane, and the rotor was synthesized. Finally, the three-dimensional complex surface of the rotor was obtained through the post-processing of the rotor point cloud. Since the rotors are far away from the rotorcraft body, the rotorcraft body should be simplified appropriately. Moreover, the relative positional relationship of the rotors should be strictly controlled to establish the overall grid model in the hovering state. To ensure the accuracy of the downwash flow field calculation, the number of grids finally reached 5.218 million. Figure 2f shows the structured grid distribution for the surface of the critical component rotor.

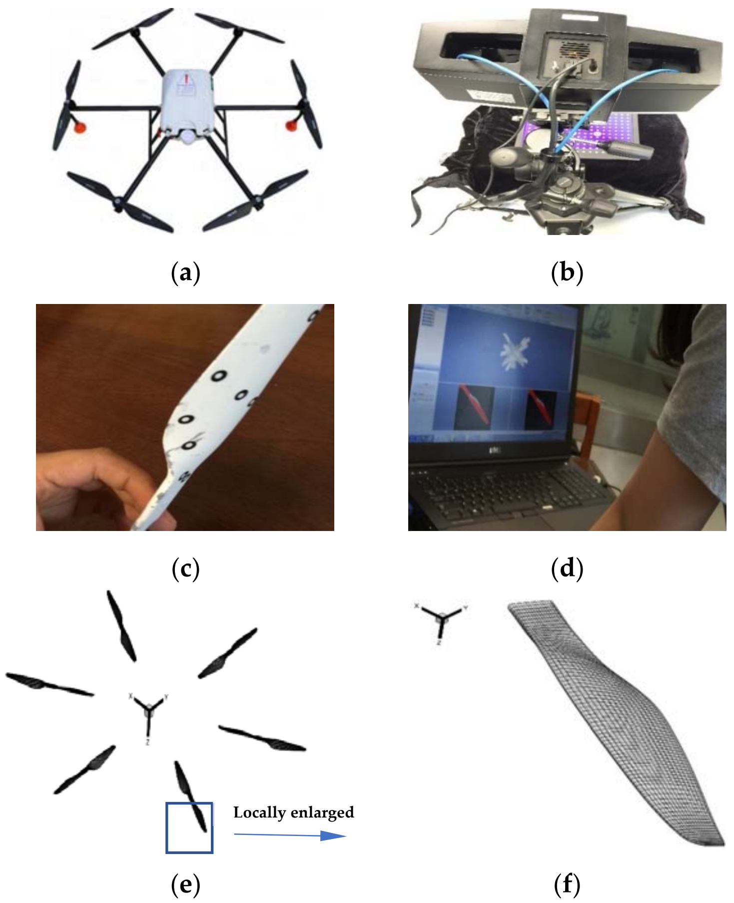

Figure 2. Scanning and reconstruction of crucial components of multi-rotor plant protection UAV: (**a**) Airframe structure of multi-rotor plant protection UAV; (**b**) Optimscan5-2015011K05 scanner; (**c**) Closely markers in places with significant curvature changes; (**d**) Synthesis of multi-angle surface point clouds by a team member; (**e**) Schematic diagram of wall structured mesh for vital components; (**f**) Partially enlarged view of the structured mesh model of the rotor component.

2.2. Governing Equations of the Downwash Flow Field

The Navier–Stokes equation is used as the governing equation in the downwash area of the rotor, to accurately calculate the influence of viscosity on the aerodynamic characteristics of the rotor. Compared with the fixed (inertial) coordinate system, the Reynolds-averaged Navier–Stokes equation in the non-inertial coordinate system is added as a source term due to the rotation, and the governing equation in the conservative integral form can be written [27]:

$$\frac{\partial}{\partial t}\iiint\limits_{\partial V}\vec{\boldsymbol{W}}dV+\iint\limits_{\partial S}\left(\vec{\boldsymbol{F}}-\vec{\boldsymbol{G}}\right)\cdot\vec{n}\,dS=\iiint\limits_{\partial V}\vec{\boldsymbol{Q}}dV \tag{1}$$

$$\vec{W} = \begin{bmatrix} \rho \\ \rho u \\ \rho v \\ \rho\omega \\ \rho E_r \end{bmatrix}, \vec{F} = \begin{bmatrix} \rho(\vec{q} - \vec{q}_w) \\ \rho u(\vec{q} - \vec{q}_w) + p\vec{i}_x \\ \rho v(\vec{q} - \vec{q}_w) + p\vec{i}_y \\ \rho\omega(\vec{q} - \vec{q}_w) + p\vec{i}_z \\ \rho H(\vec{q} - \vec{q}_w) \end{bmatrix}, \vec{G} = \begin{bmatrix} 0 \\ \tau_{xx}\vec{i}_x + \tau_{yx}\vec{i}_y + \tau_{zx}\vec{i}_z \\ \tau_{xy}\vec{i}_x + \tau_{yy}\vec{i}_y + \tau_{zy}\vec{i}_z \\ \tau_{xz}\vec{i}_x + \tau_{yz}\vec{i}_y + \tau_{zz}\vec{i}_z \\ \phi_x\vec{i}_x + \phi_y\vec{i}_y + \phi_z\vec{i}_z \end{bmatrix}, \vec{Q} = \begin{bmatrix} 0 \\ -\rho\omega\Omega \\ 0 \\ \rho u\Omega \\ 0 \end{bmatrix}$$

where S is the surface area of the control body; V is the volume of the control body; the first term $\vec{W}$ in the equation is the conserved variable; the second term ($\vec{F}$–$\vec{G}$) in the equation is the difference between inviscid flux and viscous flux; the third term $\vec{Q}$ is the flux due to rotor rotation; E_r, H_r, and Q are total internal energy, total enthalpy, and rotational angular velocity vector, respectively; ϕ_x, ϕ_y, and ϕ_z are sticky terms in three directions; and $\vec{q}$ and $\vec{q}_w$ denote absolute speed and implicated speed.

2.3. Turbulence Model and Solution Method of Downwash Airflow

The realizable k-ε turbulence model [28], which is more suitable for large shear flow, was specially adopted in this study. The governing equations are discretized by the finite volume method, and then the pressure-based solver is used for transient calculation. To ensure the stability and convergence of the analysis, the second-order coupling scheme is selected for iterative calculation.

The roadmap of this study is shown in Figure 3.

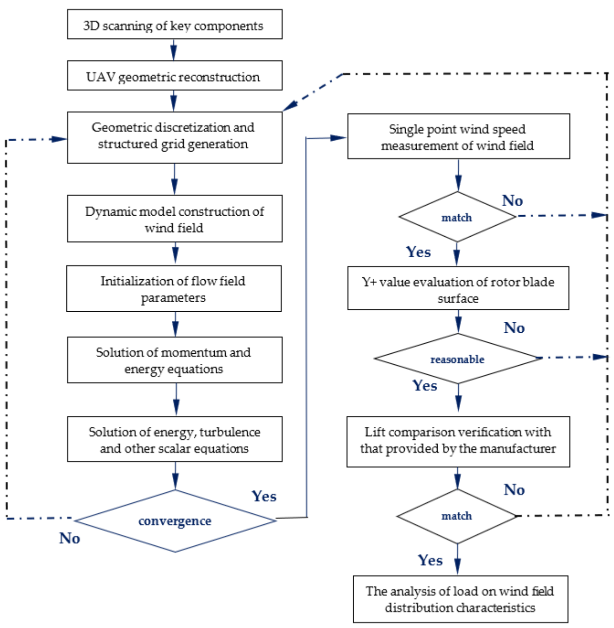

Figure 3. Workflow of this article.

3. Study on the Influence of Load on the Distribution of Downwash Flow Field

3.1. Reliability Verification of Numerical Calculation for Downwash Flow Field

To compare and obtain a robust and reliable analysis of downwash airflow, reliability verification of numerical calculation for downwash is necessary before the study on the influence of load on the distribution of downwash. In this research, the downwash test data in the hovering state and the rotor pulling force test under different loads have been strongly supported by Xi'an Wideworldz Aviation Science and Technology Co., Ltd. (Xi'an, China).

Downwash, as we know, is the critical factor affecting the deposition level of multi-rotor plant protection UAVs. However, what we use most is the vertical Z-direction velocity of the downwash air flow of the UAV. We verified the calculation reliability of the vertical velocity of the downwash under 1kg load condition in this section. The wind speed feature points were set under each rotor, the heights of the observation points from the rotor were 1 m and 2 m, respectively, and the wind speed test was carried out on a sunny day with light wind. The flight hover preparation (Figure 4a), the downwash airflow wind test at two altitudes in hover (Figure 4b), the z-direction velocity distribution for longitudinal section of wind calculation (Figure 4c), the comparison of relative errors between theoretically calculated values and experimental values of z-velocity at 12 monitoring points (Figure 4d), and the y+ (Figure 4e) of rotor wall for theoretical calculation are all presented in Figure 4. In addition, the comparison of calculated and designed values for rotor lifts in different load conditions is listed in Table 1. As can be seen, the maximum relative error of the wind speed at each observation point was about 11%, the y+ of each rotor wall did not exceed 20, and the calculated value of the rotor lifts were very close to the design values. Overall, the numerical calculation accuracy of the downwash met the requirements of the subsequent detailed analysis.

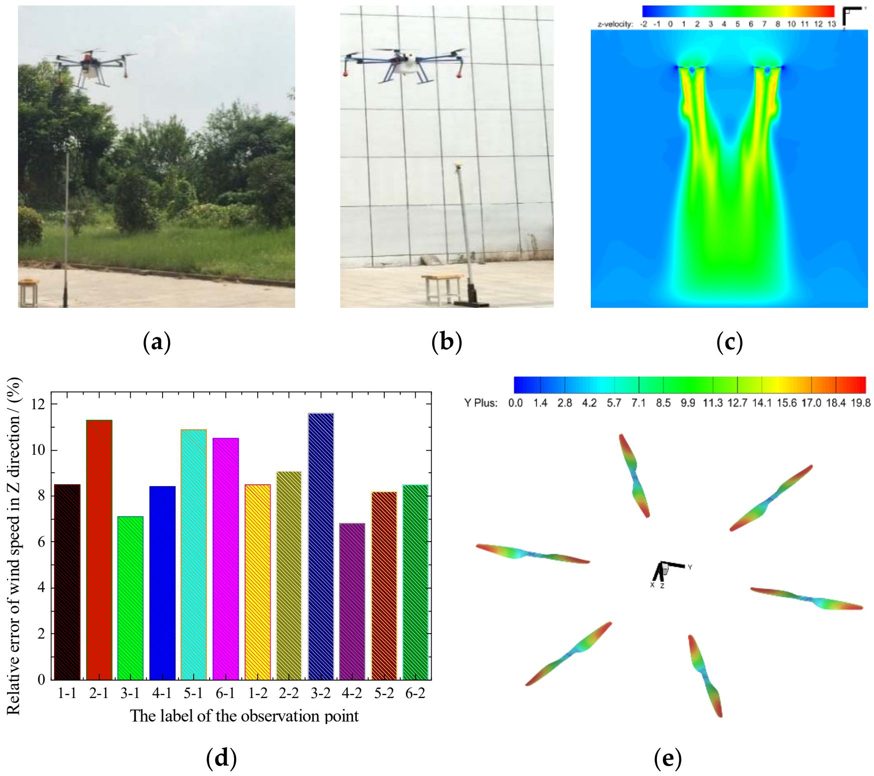

Figure 4. Reliability verification of wind field model: (**a**) Wind speed test preparation; (**b**) Test of z-direction speed under the rotor; (**c**) Calculation cloud map of z-direction velocity of the longitudinal section below rotor; (**d**) Relative error of z-velocity calculation and test; (**e**) The y+ cloud map of the rotor wall after the wind field calculation is stabilized.

Table 1. Comparison of calculated and designed values for rotor lifts in different load conditions.

Load (kg)	Simulated Lift Values of Single Rotors (N)						Total Simulated Lift (N)	Total Designed Lift (N)
	Rotor 1	Rotor 2	Rotor 3	Rotor 4	Rotor 5	Rotor 6		
0	9.8827	9.8813	9.8805	9.8755	9.8738	9.8675	59.2613	58.8
1	11.5341	11.5359	11.5311	11.5358	11.5276	11.5263	69.1908	68.6
2	13.0190	13.0234	13.0279	13.0184	13.0150	13.0049	78.1086	78.4
3	14.6091	14.6117	14.6063	14.6111	14.5991	14.5974	87.6347	88.2
4	16.3081	16.3037	16.3053	16.3077	16.2957	16.2952	97.8157	98.0
5	17.9452	17.9497	17.9487	17.9448	17.9453	17.9487	107.6824	107.8

3.2. Effect of Load on Longitudinal and Transverse Wind Speed Distribution of Downwash

Based on the above theoretical calculation methods, the unsteady numerical calculations of the hovering downwash under different loads were carried out. A total of 6 working conditions under each load were respectively calculated for 3.005 s, 3.032 s, 3.035 s, 3.095 s, 3.054 s, and 3.005 s. The parallel calculation was carried out on the HP Z840 workstation (HP, Palo Alto, CA, USA), the calculation time of each working condition was about 18 days, and the final downwash airflow was basically in a dynamic and stable state.

It could be seen by combining Figures 4c and 5b that the speed in the vertical z direction was the most significant proportion of the absolute velocity. It is worth mentioning that the vertical z-direction downwash was used to press down the droplets and shake the canopy, thereby increasing the droplet deposition amount and deposition uniformity. In terms of the differences between multi-rotor plant protection UAVs and other plant protection machineries, the above-mentioned point was the most important. Velocity distributions of the ZOY plane for downwash airflow under six load conditions are presented in Figure 5. As can be seen, due to passing through the geometric centers of the two rotors on the opposite side, the velocity distribution of the ZOY plane presented a completely symmetrical law. As an extension, it can be concluded that the greater the load, the higher the maximum wind speed, and the maximum wind speeds of the six conditions in the ZOY plane were 9.1, 9.9, 10.5, 11.1, 11.8, 12.3 m/s, respectively. In addition, Bernoulli's equation shows that the higher the wind speed, the lower the pressure. As a result, under the induction of the high-speed rotation of the rotor, the wind speed-affected area of the ZOY section in Figure 5 shows the characteristics of alternating contraction and expansion.

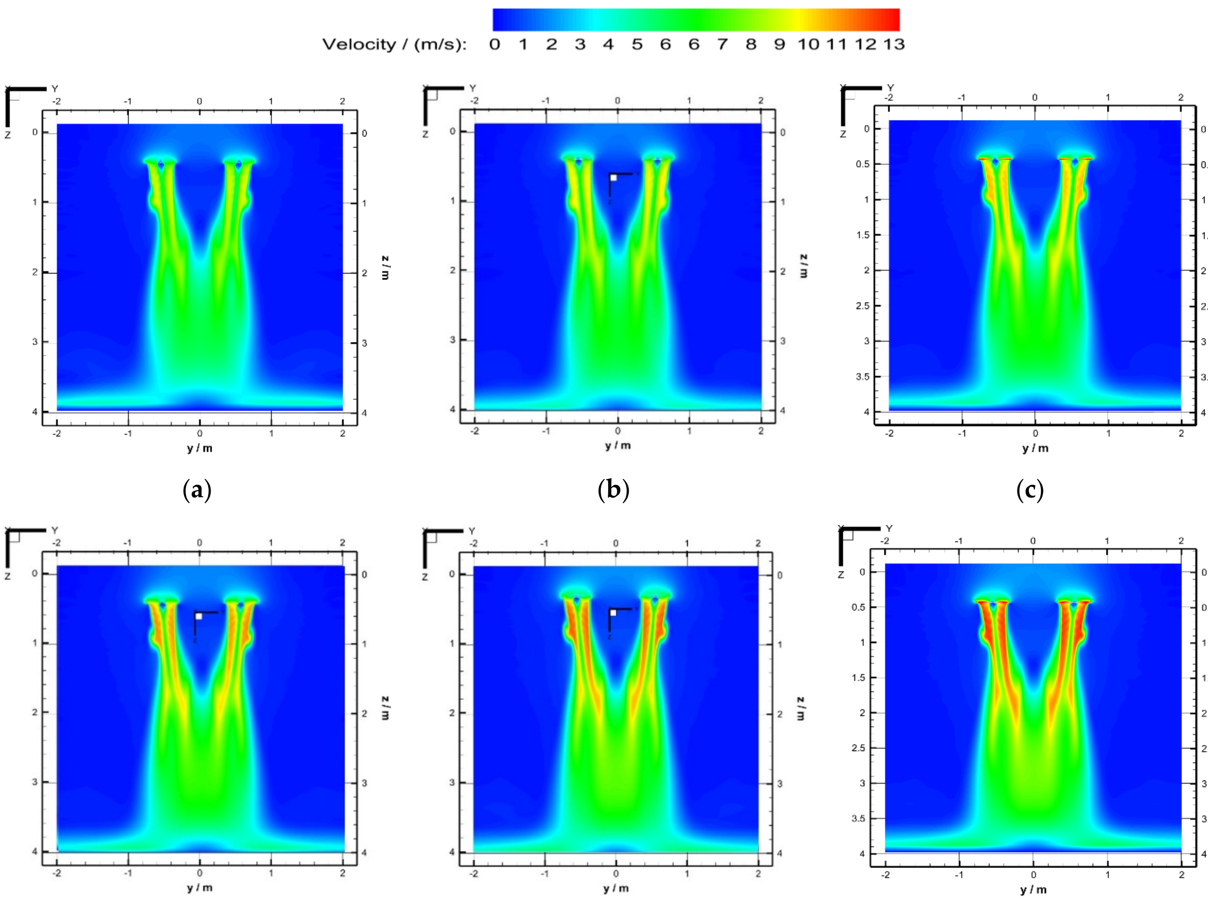

(**a**) (**b**) (**c**)

(**d**) (**e**) (**f**)

Figure 5. Velocity distribution of the ZOY planes of different pesticide load: (**a**) 0 kg; (**b**) 1 kg; (**c**) 2 kg; (**d**) 3 kg; (**e**) 4 kg; (**f**) 5 kg.

Velocity distributions of the ZOX plane for downwash under six load conditions are displayed in Figure 6. As can be seen, the airflow velocity is significantly lower in the XOZ section between the rotors compared to the YOZ section, and the maximum wind speeds of the six conditions in the ZOX plane were 6.14, 6.57, 7.12, 7.75, 8.40, 8.70 m/s. What is more, from the working principle of the multi-rotor plant protection UAV in Figure 2a, we know that the rotation directions of the adjacent rotors were opposite, to maintain the air balance of the UAV body and complete the flight action. However, adjacent rotors might rotate inward or outward simultaneously, which made the aerodynamic interference between rotors very strong. As a result, the inter-wing interference effect made the downwash velocity value asymmetry in this ZOX section obvious, which meant that the wind speed on the positive side of the *x*-axis was significantly larger than the corresponding value in the negative direction of the *x*-axis. Therefore, there was an independent peak area of wind speed in the "rotating inward area" before the downwash flows of each rotor met. What is more, the load had a significant influence on the distribution of the downwash area for the XOZ section, which is that the larger the load and the rotor speed, the more serious the inter-wing interference phenomenon. Finally, by comparing Figure 6a–f, it could be seen that the peak area of wind speed in the "rotating inward area" was constantly moving outside.

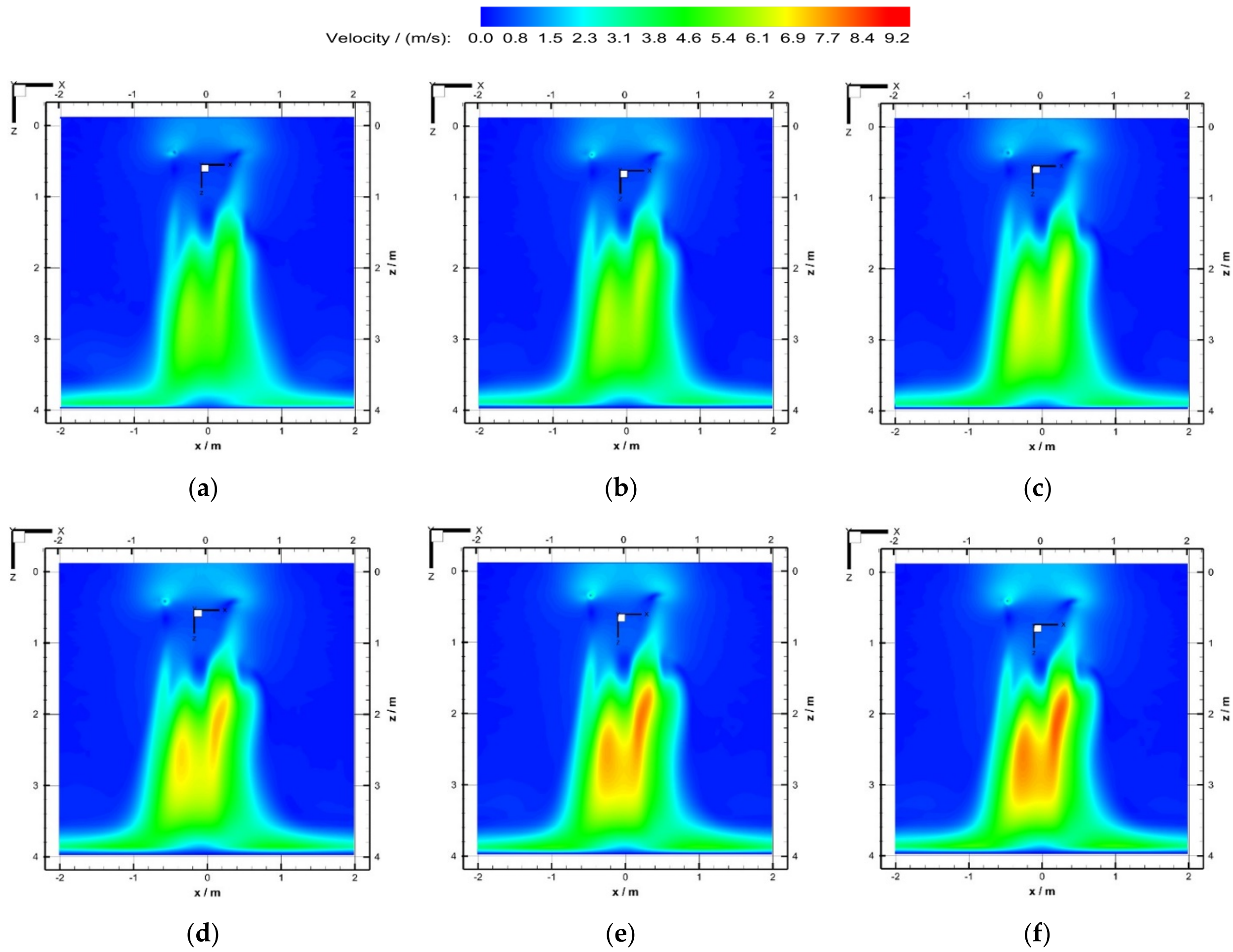

Figure 6. Velocity distribution of the ZOX planes of different pesticide load: (**a**) 0 kg; (**b**) 1 kg; (**c**) 2 kg; (**d**) 3 kg; (**e**) 4 kg; (**f**) 5 kg.

As is known, farmers pay more attention to the deposition quality of the upper, middle, and lower layers of the crop canopy, which is directly related to the wind speed distribution in each cross-section (XOY section) of the downwash airflow. Due to the limitations of space, and to analyze the velocity attenuation law of the cross-section in more detail, this study only gave the wind speed distribution results of the XOY section for the two load conditions in Figure 7. As can be seen, the development and attenuation laws of the velocity distribution on the cross-section were almost the same for the two conditions of the 0 kg load (Figure 7a–f) and the 4 kg load (Figure 7g–l). In contrast, the velocity values of the cross-section at the same height were quite different. Moreover, under the combined influence of strong shear effect caused by high-speed rotor rotation and the dissipation effect caused by air viscosity, the high-speed area of the cross-section at each height was gradually dissipated from the six areas into one focused area, and the wind speed of the center is higher than that of the periphery. It should be mentioned that such a conclusion can be drawn from the analysis of Figure 7e,f,k,l that the downwash flow developed into a focused circle on the cross-section after the rotor was about 2.5 m (the Z coordinate of the rotor is 0.425 m) off the ground. It indicated that the flying spray height of this UAV was recommended to be 2.5 m or higher if flight safety could be ensured. As an extension, the distance between the rotor plane and the focused circle was an excellent spray height only when the influence area of the downwash was dissipated into the focused circle.

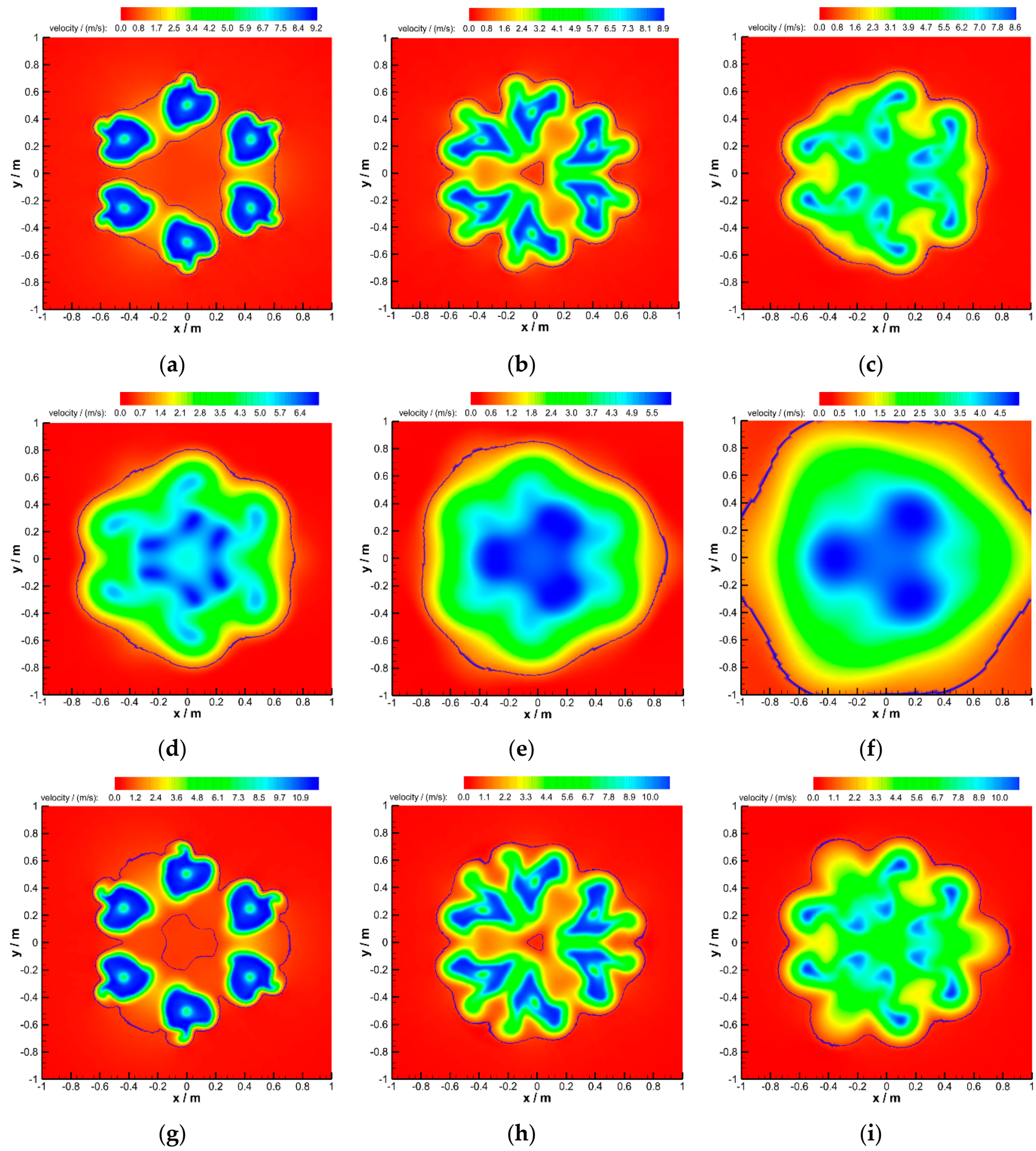

Figure 7. *Cont.*

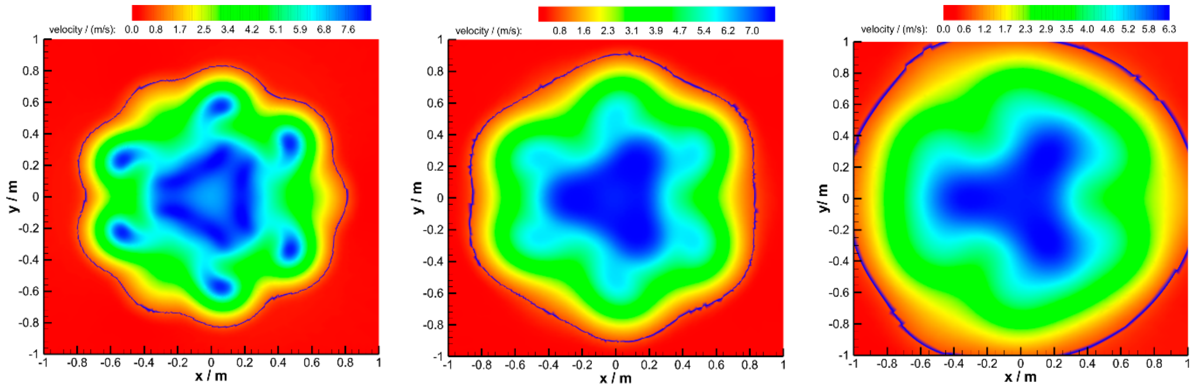

(j) (k) (l)

Figure 7. Velocity distribution of the XOY cross-sections for downwash airflow under different loads: (**a**) Load of 0 kg at z = 0.926 m plane; (**b**) Load of 0 kg at z = 1.426 m plane; (**c**) Load of 0 kg at z = 1.926 m plane; (**d**) Load of 0 kg at z = 2.426 m plane; (**e**) Load of 0 kg at z = 2.926 m plane; (**f**) Load of 0 kg at z = 3.426 m plane; (**g**) Load of 4 kg at z = 0.926 m plane; (**h**) Load of 4 kg at z = 1.426 m plane; (**i**) Load of 4 kg at z = 1.926 m plane; (**j**) Load of 4 kg at z = 2.426 m plane; (**k**) Load of 4 kg at z = 2.926 m plane; (**l**) Load of 4 kg at z = 3.426 m plane.

3.3. Effect of Load on Flow Characteristics of Downwash

In general, the lateral flow characteristics of the downwash airflow (especially the downwash area near the rotor) have a direct impact on the movement and deposition laws of the droplets. The lateral flow characteristics of the cross-section for downwash under the load condition of 3 kg are shown in Figure 8, and the velocity distribution of the XOZ plane (adjacent rotors) at various heights under different loads are plotted in detail in Figure 9. As can be seen from Figure 8, three "airflow inlet" and three "airflow outlet" regions were formed on the XOY section due to the opposite rotation of adjacent rotors. Furthermore, the downwash area was divided into three areas that were symmetrically distributed at 120 degrees. The velocity streamlines of the cross-section in the pressure background are presented in Figure 8b. As can be seen, the pressure in the affected area of the downwash airflow was significantly lower than that in the geometric center area and the peripheral area of the downwash. This was mainly because that the "airflow inlet" introduced the airflow into the geometric center area and caused an increase in air pressure. Then, the airflow flowed out from the geometric center through the "airflow outlet" area, and the external pressure being greater than that of the "airflow outlet", resulted in the formation of an apparent vortex dissipation phenomenon in the three symmetrical "airflow outlet" areas. Finally, the wind speed at the "airflow outlet" was significantly reduced relative to the wind speed at the "airflow inlet" under the influence of vortex dissipation. Given this, the speed distributions between adjacent rotors of the typical heights are plotted in detail in Figure 8. As the vertical distance from the rotor was farther, the shear-induced effect of high-speed rotation became weaker and weaker, and the flow speed difference between "airflow inlet" and "airflow outlet" became smaller and smaller under the influence of air viscosity. As a result, combined with Figures 7k, 8b and 9c, the difference in flow speed between "airflow inlet" and "airflow outlet" was already very minimal when the vertical distance from the rotor reached 2.5 m. It is worth mentioning here that through the previous analysis, we recommend that the multi-rotor plant protection UAV fly along the x-direction: the nozzles are installed directly under the two rotors along the y-direction (the geometric center coordinates of the rotor plane are (0, 0, 0.425)), the centrifugal nozzle with positive *y*-axis rotates counterclockwise, and the centrifugal nozzle with negative *y*-axis rotates clockwise, and the spray height is initially set at 2.5 m.

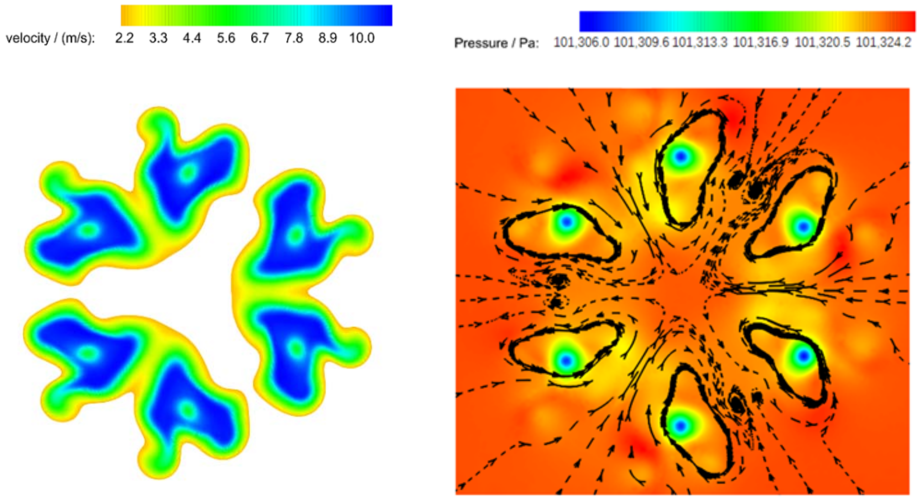

(**a**) (**b**)

Figure 8. Cloud map of lateral flow characteristics for 3 kg load working condition at different heights: (**a**) Velocity distribution at z = 1.426 m; (**b**) Streamline diagram on the background of pressure at z = 0.926 m.

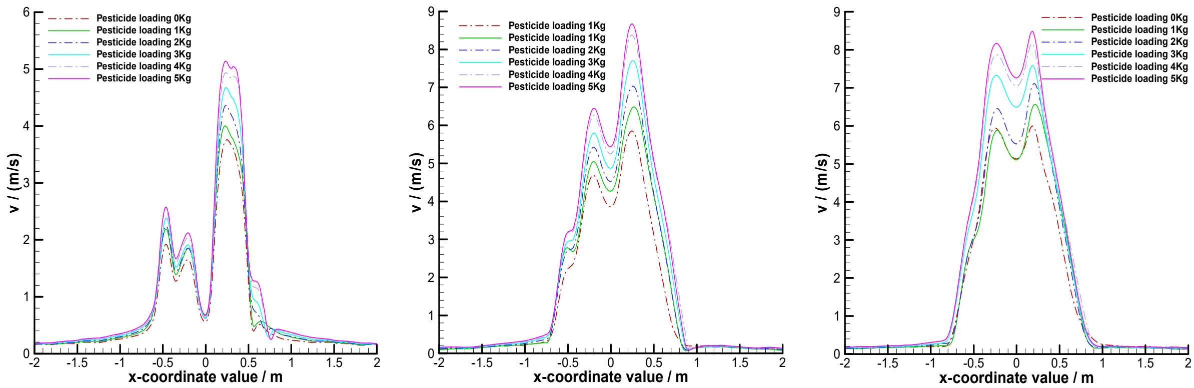

(**a**) (**b**) (**c**)

Figure 9. Velocity distribution of the xoz plane (adjacent rotors) at various heights: (**a**) z = 1.426 m; (**b**) z = 1.926 m; (**c**) z = 2.426 m.

To study the development and dissipation law of downwash airflow more intuitively, velocity distributions at various key longitudinal lines under different loads are shown in Figure 10. As seen in Figure 10a, the speed on the longitudinal line at the geometric center of the UAV showed a trend of decreasing, then increasing, and finally decreasing to 0. It is worth mentioning that this trend corresponded to the feature of first contraction and then expansion of the affected area for the downwash velocity in Figure 5, and the height at which this maximum speed occurred was also in line with our recommended reasonable spraying height (the appropriate height of the rotor above the ground was about 2.5 m). Combined with Figures 5 and 10b, the maximum wind speed of the downwash was not directly below the rotor, but at the middle of the half-rotor length near the wingtip. Therefore, due to the feature of contraction and expansion of the affected area for the downwash velocity in Figure 5, the wind speed directly below the rotor showed a trend of increasing, then decreasing, then increasing, and finally decreasing to 0. Figure 8b showed that the "airflow inlet" was only affected by the airflow flowing into the geometric center from the periphery, while the "airflow outlet" was affected by the combined effect of two airflows flowing from the periphery into the geometric center and from the geometric center into the periphery. As a result, the air velocity below the inlet showed a simple trend of rising and then decaying to 0, while the air velocity below the outlet presented a complex oscillation trend.

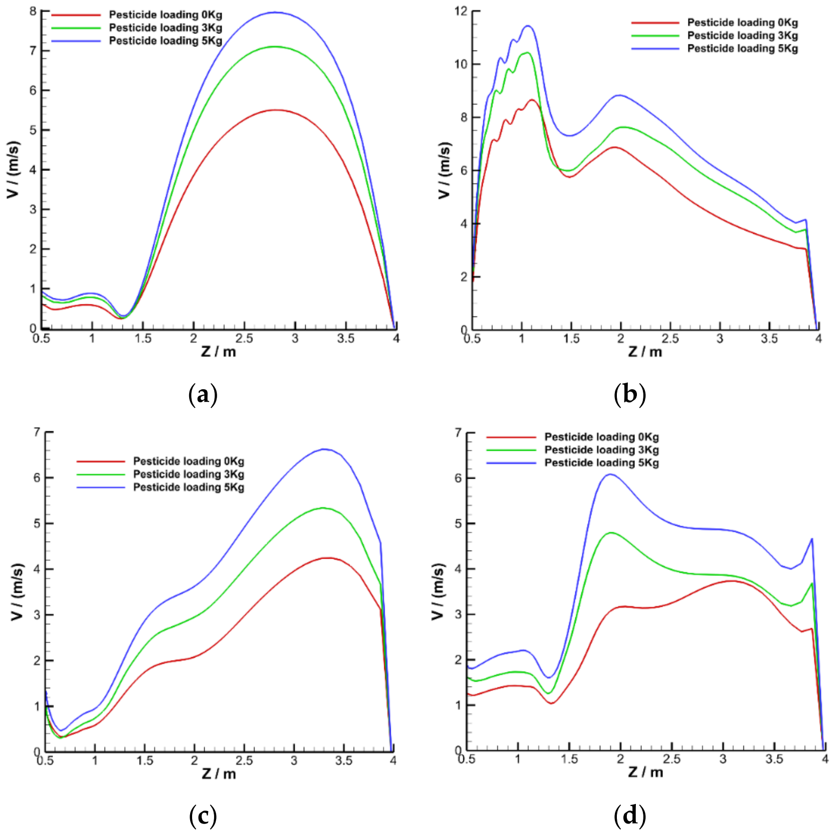

Figure 10. Velocity distribution at various longitudinal line under the different loads: (**a**) Longitudinal line at the geometric center of the UAV; (**b**) Longitudinal line at the geometric center of the rotor; (**c**) Longitudinal line at the airflow inlet of the adjacent rotors; (**d**) Longitudinal line at the airflow outlet of the adjacent rotors.

From the perspective of the development trend of plant protection machinery, multi-rotor plant protection Unmanned Aerial Vehicles (UAVs) have good terrain adaptation ability and efficient ultra-low altitude spraying capacity, and have become an important development direction of efficient plant protection equipment. However, the interaction mechanisms of wind field, droplet, and crop are unclear, which has become the bottleneck factor restricting the improvement of the deposition distribution quality; wind field research under different loads is an important part of the solution. Therefore, the research in this paper can provide guidance for the prediction of the droplet drift distance of aerial pesticide application. This paper can also lay a foundation for the study on the influence mechanism of wind field, droplet, and crop interaction on the canopy deposition based on the multi-rotor plant protection UAV.

4. Conclusions

This study was motivated by attaining a detailed understanding of velocity distributions and flow characteristics of downwash for multi-rotor plant protection UAVs under different pesticide loads, and then making recommendations for the formulation of spray strategies. Our attempts explored the application of the second-order coupling scheme based on the pressure-based solver to calculate the unsteady downwash flow field, combined with the test verification. Based on the wind speed distribution law of each typical longitudinal section and the flow characteristics of each transverse section under different load conditions, we give the following discussions:

(1) The errors between the calculated and the experimental values of wind speed in the vertical direction for the critical observation points were within 11%, the calculated values of the rotor pulling force were in good agreement with the design values, and the y+ value of the rotor wall was within a reasonable range.
(2) Spray height of this multi-rotor plant protection UAV was recommended to be 2.5 m or higher, and the influence area of the downwash at the height of 2.5 m was dissipated into the focused circle.
(3) The nozzles were recommended to be installed directly under the two rotors along the y-direction, the centrifugal nozzle with positive y-axis rotate counterclockwise, and the centrifugal nozzle with negative y-axis rotate clockwise, so that the droplets can be induced by the same turning rotor to the underside of the rotorcraft body and effectively dispersed. In addition, further work will focus on the influence mechanism of wind field, droplet, and crop interaction on the canopy deposition.
(4) Compared with the four-rotor plant protection UAV [29], the six-rotor plant protection UAV had obvious inter wing interference. Under the influence of wing interference caused by the opposite velocity of adjacent rotor, the turbulent effect of down wash flow was obvious, and the "airflow inlet" and "airflow outlet" region appeared between the wings area at the cross section.
(5) The results show that the pesticide load had an obvious effect on the longitudinal distribution of downwash airflow. As the load increased, the longitudinal distribution of flow field transited from "shrinkage–expansion–shrinkage" to "shrinkage–expansion".

Author Contributions: Q.C. designed the experiments. F.Y. completed the theoretical calculation. F.Y., Y.R., Q.C. and H.Z. conducted experiments and analyzed the data. F.Y. wrote the paper. L.Z. completed the English revisions. All authors have read and agreed to the published version of the manuscript.

Funding: The authors acknowledge the support provided by the National Natural Science Foundation of China (No. 52275257, No. 51705264), the Metasequoia teacher research start-up project (No. 163040148), and the help from Xi'an Wideworldz Aviation Science and Technology Co., Ltd.

Conflicts of Interest: The authors declare no conflict of interest.

References

1. Lan, Y.; Shengde, C.; Fritz, B.K. Current status and future trends of precision agricultural aviation technologies. International. *J. Agric. Biol. Eng.* **2017**, *10*, 1–17.
2. Li, J.; Lan, Y.; Shi, Y. Research progress on airflow characteristics and field pesticide application system of rotary-wing UAV. *Trans. Chin. Soc. Agric. Eng.* **2018**, *34*, 104–118.
3. States, U. Unmanned Flight: The Drones Come Home-Pictures. *National Geographic*. March 2013. Available online: https://www.nationalgeographic.com/magazine/2013/03/drones-come-home/ (accessed on 18 June 2018).
4. Su, D.; Yao, W.; Yu, F.; Liu, Y.; Zheng, Z.; Wang, Y.; Xu, T.; Chen, C. Single-Neuron PID UAV Variable Fertilizer Application Control System Based on a Weighted Coefficient Learning Correction. *Agriculture* **2022**, *12*, 1019. [CrossRef]
5. Xuemei, L.; Xinghua, L.; Huiyuan, C.; Jin, Y. Research Progress and Trend Analysis of Crop Canopy Droplet Deposition. *Trans. Chin. Soc. Agric. Mach.* **2021**, *52*, 1–20.
6. Shuping, F.; Yu, R.; Yangyang, L.; Chenming, H.; Xuyang, C.; Bin, L. Route Planning of Helicopters Spraying Operations in Multiple Forest Areas. *Forests* **2021**, *12*, 1658.
7. Yulong, N.; Huichun, Z.; Jiaqiang, Z.; Kunqi, Y.; Weikang, Y.; Meng, Z. Research on profiling tracking control optimization of orchard sprayer based on the phenotypic characteristics of tree crown. *Comput. Electron. Agric.* **2022**, *192*, 106455.
8. Dunn, A.M.; Julien, G.; Ernst, W.R.; Cook, A.; Doe, K.G.; Jackman, P.M. Evaluation of buffer zone effectiveness in mitigating the risks associated with agricultural runoff in Prince Edward Island. *Sci. Total Environ.* **2011**, *409*, 868–882. [CrossRef]
9. Craig, I.P. The GDS model-a rapid computational technique for the calculation of aircraft spray drift buffer distances. *Comput. Electron. Agric.* **2010**, *43*, 235–250. [CrossRef]
10. Qin, W.C.; Qiu, B.J.; Xue, X.Y.; Chen, C.; Xu, Z.F.; Zhou, Q.Q. Droplet deposition and control effect of insecticides sprayed with an unmanned aerial vehicle against plant hoppers. *Crop Prot.* **2016**, *85*, 79–88. [CrossRef]
11. Ahmad, F.; Qiu, B.; Dong, X.; Ma, J.; Huang, X.; Ahmed, S.; Chandio, F.A. Effect of operational parameters of UAV sprayer on spray deposition pattern in target and off-target zones during outer field weed control application. *Comput. Electron. Agric.* **2020**, *172*, 105350. [CrossRef]

12. He, Y.; Xiao, S.; Fang, H.; Dong, T.; Tang, Y.; Nie, P.; Wu, J.; Luo, S. Development situation and spraying decision of spray nozzle for plant protection UAV. *Trans. Chin. Soc. Agric. Eng.* **2018**, *34*, 113–124.
13. Wang, C.; He, X.; Wang, X.; Wang, Z.; Wang, S.; Li, L.; Bonds, J.; Herbst, A.; Wang, Z. Testing method and distribution characteristics of spatial pesticide spraying deposition quality balance for unmanned aerial vehicle. *Int. J. Agric. Biol. Eng.* **2018**, *11*, 18–26. [CrossRef]
14. Zhang, Y.; Li, Y.; He, Y.; Liu, F.; Cen, H.; Fang, H. Near ground platform development to simulate UAV aerial spraying and its spraying test under different conditions. *Comput. Electron. Agric.* **2018**, *148*, 8–18. [CrossRef]
15. Jian, Z.; Qing, C.; Minghong, S.; Hongping, Z.; Linyun, X. Interaction and influence of a flow field and particleboard particles in an airflow forming machine with a coupled Euler-DPM model. *PloS ONE* **2021**, *16*, 1–25.
16. Ling, W.; Du, C.; Mengchao, Z.; Yu, W.; Ze, Y.; Shumao, W. CFD Simulation of Low-attitude Droplets Deposition Characteristics for UAV based on Multi-feature Fusion. *IFAC Pap. OnLine* **2018**, *51*, 648–653. [CrossRef]
17. Li, J.; Shi, Y.; Lan, Y.; Guo, S. Vertical distribution and vortex structure of rotor wind field under the influence of rice canopy. *Comput. Electron. Agric.* **2019**, *159*, 140–146. [CrossRef]
18. Zhiwei, T.I.A.N.; Xinyu, X.U.E.; Yang, X.U.; Fengbo, Y.A.N.G.; Zhu, S.U.N. Effect of Plant Protection UAVs Downwash on Crop Canopy. *Trans. Chin. Soc. Agric. Mach.* **2021**, *52*, 40–48.
19. Shengde, C.H.E.N.; Yubin, L.A.N.; Bradley, K.F.; Jiyu, L.I.; Aimin, L.I.U.; Yuedong, M.A.O. Effect of Wind Field below Rotor on Distribution of Aerial Spraying Droplet Deposition by Using Multi-rotor UAV. *Trans. Chin. Soc. Agric. Mach.* **2017**, *48*, 105–113.
20. Yeo, D.; Shrestha, E.; Paley, D.A.; Atkins, E.M. An Empirical Model of Rotorcraft UAV Downwash for Disturbance Localization and Avoidance. In Proceedings of the AIAA Atmospheric Flight Mechanics Conference, Kissimmee, FL, USA, 5–9 January 2015.
21. Bludau, J.; Rauleder, J.; Friedmann, L.; Hajek, M. Real-Time Simulation of Dynamic Inflow Using Rotorcraft Flight Dynamics Coupled With a Lattice-Boltzmann Based Fluid Simulation. In Proceedings of the 55th AIAA Aerospace Sciences Meeting, Grapevine, TX, USA, 9–13 January 2017. [CrossRef]
22. Endalew, A.M.; Debaer, C.; Rutten, N.; Vercammen, J.; Delele, M.A.; Ramon, H.; Nicolaï, B.M.; Verbovena, P. Modelling pesticide flow and deposition from air-assisted orchard spraying in orchards: A new integrated CFD approach. *Agric. Forest Meteorol.* **2010**, *150*, 1383–1392. [CrossRef]
23. Salcedo, R.; Vallet, A.; Granell, R.; Garcerá, C.; Moltó, E.; Chueca, P. Euleriane Lagrangian model of the behaviour of droplets produced by an air-assisted sprayer in a citrus orchard. *Biosyst. Eng.* **2017**, *154*, 76–91. [CrossRef]
24. Ryan, S.D.; Gerber, A.G.; Holloway, A.G.L. A computational study on spray dispersal in the wake of an aircraft. *Trans. ASABE* **2013**, *56*, 847–868.
25. Zhang, B.; Tang, Q.; Chen, L.P.; Xu, M. Numerical simulation of wake vortices of crop spraying aircraft close to the ground. *Biosyst. Eng.* **2016**, *145*, 52–64. [CrossRef]
26. Zhang, B.; Tang, Q.; Chen, L.P.; Zhang, R.R.; Xu, M. Numerical simulation of spray drift and deposition from a crop spraying aircraft using a CFD approach. *Biosyst. Eng.* **2018**, *166*, 184–199. [CrossRef]
27. Gao, X.F.; Shi, W.D.; Zhang, D.S.; Zhang, Q.H.; Fang, B. Optimization Design and Test of Vortex Pump Based on CFD Orthogonal Test. *Trans. Chin. Soc. Agric. Mach.* **2014**, *45*, 101–106.
28. Niu, Y. *Research on Internal Ballistic Flow Field Characteristics of Self-Eject Launch*; Beijing Institute of Technology: Beijing, China, 2016.
29. Guo, Q.; Zhu, Y.; Tang, Y.; Hou, C.; He, Y.; Zhuang, J.; Zheng, Y.; Luo, S. CFD simulation and experimental verification of the spatial and temporal distributions of the downwash airflow of a quad-rotor agricultural UAV in hover. *Comput. Electron. Agric.* **2020**, *172*, 105343. [CrossRef]